Chinese Chemical Letters 37 (2026) 111503

Contents lists available at ScienceDirect

Chinese Chemical Letters

journal homepage: www.elsevier.com/locate/cclet

Kinetically controlled Np(VI)/Pu(IV) selective reduction by *n*-butyraldehyde

Xiaobo Li[a], Qunyan Wu[a,*], Congzhi Wang[a], Jianhui Lan[a], Meng Zhang[b], Weiqun Shi[a,c,*]

[a] Laboratory of Nuclear Energy Chemistry, Institute of High Energy Physics, Chinese Academy of Sciences, Beijing 100049, China
[b] Fundamental Science on Nuclear Safety and Simulation Technology Laboratory, College of Nuclear Science and Technology, Harbin Engineering University, Harbin 150001, China
[c] Institute of Nuclear Fuel Cycle and Materials, School of Mechanical Engineering, Shanghai Jiao Tong University, Shanghai 200240, China

ARTICLE INFO

Article history:
Received 13 January 2025
Revised 9 June 2025
Accepted 24 June 2025
Available online 1 July 2025

Keywords:
Neptunium
Plutonium
Reduction
Density functional theory
Kinetic control

ABSTRACT

The demand for ^{238}Pu (nuclear battery heat source) drives the separation of its precursor, ^{237}Np, from spent nuclear fuel (SNF). However, the co-existence of multi-valence states (IV/V/VI) of Np and similar redox behavior with Pu(IV) hinder the effective separation of Np. *N*-Butyraldehyde (*n*-C_3H_7CHO) selectively reduces Np(VI) to Np(V) without reducing Pu(IV). Herein, we examined the reduction mechanisms of Np(VI) and Pu(IV) by *n*-C_3H_7CHO using relativistic density functional theory. Based on the results of the potential energy profiles, the reductions of both Np(VI) and Pu(IV) by *n*-C_3H_7CHO are thermodynamically feasible, whereas only the former is kinetically achievable. It uncovers that *n*-C_3H_7CHO can only reduce Np(VI) to Np(V) owing to kinetically controlled selective reduction. The analyses of spin density and bond distance indicate that the reduction nature for the first Np(VI)/Pu(IV) belongs to hydrogen atom transfer, whereas that for the second one involves outer-sphere electron transfer. Localized molecular orbitals (LMOs) analysis discloses the bonding evolution during the reduction process of Np(VI)/Pu(IV). This study elucidates the reason behind the kinetically controlled selective reduction of Np(VI)/Pu(IV) by *n*-C_3H_7CHO at the molecular level and offers in-depth perspectives on the isolation of specific metal ions from the view of kinetic control.

© 2025 Published by Elsevier B.V. on behalf of Chinese Chemical Society and Institute of Materia Medica, Chinese Academy of Medical Sciences.

To achieve the sustainable development of nuclear energy, it is inevitable to perfect and improve the spent fuel reprocessing process [1–3]. The current commercialized Plutonium Uranium Reduction EXtraction (PUREX) only achieves uranium (U)/plutonium (Pu) separation. Neptunium (Np) in spent nuclear fuel (SNF) is not separated and enters into high-level liquid waste (HLLW) [4], which is vitrified and deep-buried underground. The half-life of ^{237}Np is 2.144 million years, which poses a very stringent challenge to the conditions of geological storage. In addition, ^{237}Np is the raw material for ^{238}Pu, which is commonly used in the manufacture of nuclear batteries. Nuclear batteries have very important applications in aerospace, medical, and other fields [5]. As a result, it is crucial and urgent to remove Np from SNF. In the PUREX process [6,7], the extractant tributyl phosphate (TBP) has different extraction abilities for Np in different valence states (Np(V) << Np(IV) < Np(VI)) [8–10]. Np(VI) can be reduced to Np(V) by salt-free reagents and Np(V) [11] enters into the aqueous phase, which achieves the separation of Np. Various salt-free reagents have been explored in experiments for the reduction of Np(VI), including hydroxylamines [12–16], ureas [17–19], oximes [20–23], hydrazines [24–31], and aldehydes [32–36].

Among these reductants, hydroxylamines, ureas, oximes, and isobutyraldehyde are able to reduce Np(VI) into Np(V) and Pu(IV) into Pu(III), respectively, leading to the entry of both Np and Pu together into the aqueous phase. Marhenko *et al.* studied the reduction reactions of Np(VI) and Pu(IV) with hydroxylamine in 0.33 mol/L HNO_3 solution containing U(VI) and some fission products at 60 °C and found that hydroxylamine is able to reduce Pu(IV) into Pu(III) as well as reduce Np(VI) into Np(V) and Np(IV) [16]. Dihydroxyurea achieves U/Pu separation by reducing Pu(IV) to Pu(III) [17] and accomplishes U/Np separation by reducing Np(VI) to Np(V) [18]. Koltunov *et al.* reported that acetaldoxime reduces Pu(IV)/Np(VI) to Pu(III)/Np(V), respectively, and both Pu and Np are removable from the 30% TBP/*n*-dodecane with the presence of U(VI) [20]. Uchiyama *et al.* discovered that isobutyraldehyde is capable of reducing Pu(IV)/Np(VI) to Pu(III)/Np(V) respectively without reducing U(VI), making it suitable for the Pu(IV) reduction in the U/Pu separation stage [32]. Some hydrazine deriva-

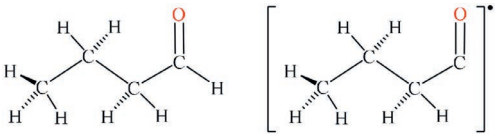
* Corresponding authors.
E-mail addresses: wuqy@ihep.ac.cn (Q. Wu), shiwq@sjtu.edu.cn (W. Shi).

https://doi.org/10.1016/j.cclet.2025.111503
1001-8417/© 2025 Published by Elsevier B.V. on behalf of Chinese Chemical Society and Institute of Materia Medica, Chinese Academy of Medical Sciences.

tives and *n*-butyraldehyde are only capable of reducing Np(VI) to Np(V) without accomplishing the reduction of Pu(IV), thus achieving sole separation of Np [24,26,30–32,34]. The obvious difference in reduction rates between Np(VI) and Pu(IV) with hydrazine or methylhydrazine can be applied for the separation of Np from Pu [30,31]. Furthermore, increasing the concentration of reductants and nitric acid as well as raising the temperature are beneficial for Np/Pu separation in the single-stage extraction experiment [30,31]. Uchiyama and colleagues demonstrated that *n*-butyraldehyde is capable of reducing Np(VI) to Np(V) without affecting Pu(IV) in 3 mol/L HNO_3 solution, thus successfully separating nearly 99.98 % of Np in the organic phase [32], which can achieve the selective reduction of Np(VI) by *n*-butyraldehyde. Subsequently, they investigated the kinetics for the reduction of Np(VI) with *n*-butyraldehyde in HNO_3 solution and 30 % TBP/*n*-dodecane and obtained the corresponding equation of reduction rate [33,36]. Based on the different reduction abilities of Np(VI) and Pu(IV) by reductants, an advanced PUREX process, known as the Partitioning Conundrum Key (PARC) process, was developed for the sole separation of Np [34]. Flow sheet experiments demonstrate that *n*-butyraldehyde selectively reduces Np(VI) to Np(V) without being affected by the coexistence of U(VI) and Tc(VII) species [34]. However, the different reduction abilities of Np(VI) and Pu(IV) by *n*-butyraldehyde have not been clearly elucidated in experiments due to the constraints of the experimental operating conditions of Np and Pu, so the theoretical study on their reduction mechanisms is very necessary.

We have conducted theoretical investigations into the reduction process of Np(VI) with hydrazine and related derivatives [37–44], revealing that the quick reduction of Np(VI) with phenylhydrazine and hydrazinopropionitrile thanks to delocalized π electrons and σ-π hyperconjugation effect, respectively [39,41]. In addition, the reduction mechanism of Pu(IV) by acetaldoxime has been clarified by the analyses of the structures and energy barriers [45]. Herein, we further investigated the reduction process and mechanism of Np(VI)/Pu(IV) using *n*-butyraldehyde as well as explained the reason behind the selective reduction of Np(VI), utilizing relativistic density functional theory. This work elucidates the structures and mechanisms of Np(VI) and Pu(IV) reduction by *n*-butyraldehyde and provides theoretical support for the application of *n*-butyraldehyde to the separation of Np/Pu in SNF.

The B3LYP hybrid functional [46,47], which can provide reliable results for studying actinide compounds [48–54], was combined with the conductor-like polarizable continuum model (CPCM) [55,56] in the Gaussian 16 software [57]. The 6–31G(d) basis set was used for C, O, N, and H atoms, the relativistic effective core potentials (RECPs) [58] replacing 60 core electrons and ECP60MWB-SEG valence basis set [59,60] were used for Np and Pu atoms. The spin-unrestricted method was employed to optimize the structures of all Pu(IV/III) and Np(VI/V) complexes, their ground states are the doublet Np(VI), triplet Np(V), quintet Pu(IV), and sextet Pu(III), respectively. Frequency calculations were performed at the same level of theory to ensure initial complexes (ICs), intermediates (INTs), and transition state (TS). The intrinsic reaction coordinate (IRC) approach was utilized to confirm the connectivity of TSs with ICs and INTs. Additionally, the Pu(IV/III) and Np(VI/V) complexes have 5f-electrons, and their energies may be sensitive to the spin-orbit coupling (SOC) effect. Previous studies have shown that the SOC effect significantly impacts the reaction energy for the systems bearing Np [61] and Pu [62]. To evaluate the influence of the SOC effect on potential energy profiles (PEPs) of Np(VI)/Pu(IV) reduction using *n*-butyraldehyde, single point calculations including SOC effect with the exact two-component (X2C) relativistic Hamiltonian within the X2C formalism [63] were performed using the B3LYP functional and all-electron Slater-type orbital (STO) triple-ζ polarized (TZ2P) basis set [64] without frozen core approximation in the Amsterdam Modeling Suite 2022 (AMS 2022) package [65–67]. The above calculations also considered the solvent effect using the Conductor-like Screening Model (COSMO) approach with Klamt's radii in the aqueous phase [68–70]. The PEPs with and without SOC effects in Fig. S1 (Supporting information) show that the SOC effect has a significant influence on the energy barrier. Thus, PEPs with SOC effect were used in the following discussion. Localized molecular orbitals (LMOs) [71] based on the optimized structures were analyzed with the Multiwfn software [72,73] to investigate the bonding evolution throughout the reaction. Spin density can clarify the change of the oxidation state of Np/Pu and elucidate the reduction nature. Independent gradient model based on Hirshfeld partition (IGMH) is used to reveal intermolecular interaction [74]. Scheme 1 illustrates the structures of *n*-butyraldehyde and its associated free radical participating in the reaction process. In addition, to assess the effect of functional on the molecular geometries, the structures of $[Np^{VI}O_2(H_2O)_5]^{2+}$, $[Np^{V}O_2(H_2O)_5]^{+}$, $[Pu^{IV}(NO_3)_2(H_2O)_7]^{2+}$, *n*-$C_3H_7CHO$ and [*n*-C_3H_7CO]$^{\bullet}$ were optimized using hybrid B3LYP and pure PBE functionals with 6–31G(d) basis set in the aqueous phase. The values of the bond distance in Fig. S2 (Supporting information) indicate that the structures are not sensitive to the functionals. So the results we discussed below are based on the B3LYP functional.



Scheme 1. Structures of *n*-C_3H_7CHO and free radical [*n*-C_3H_7CO]$^{\bullet}$.

The total reduction reaction of Np(VI)/Pu(IV) by *n*-butyraldehyde with the participation of a water molecule is shown in Eq. 3. The possible reaction processes are shown in Eqs. 2 and 3. In 3 mol/L HNO_3 solution, $[Pu^{IV}(NO_3)_2(H_2O)_7]^{2+}$ and $[Np^{VI}O_2(H_2O)_5]^{2+}$ represent the dominant species for Pu(IV) [75–78] and Np(VI) [79–81], respectively, so they were used as reactants of the reduction reactions of Pu(IV) and Np(VI). The free radical [*n*-C_3H_7CO]$^{\bullet}$ is likely to exist in certain conditions [82,83].

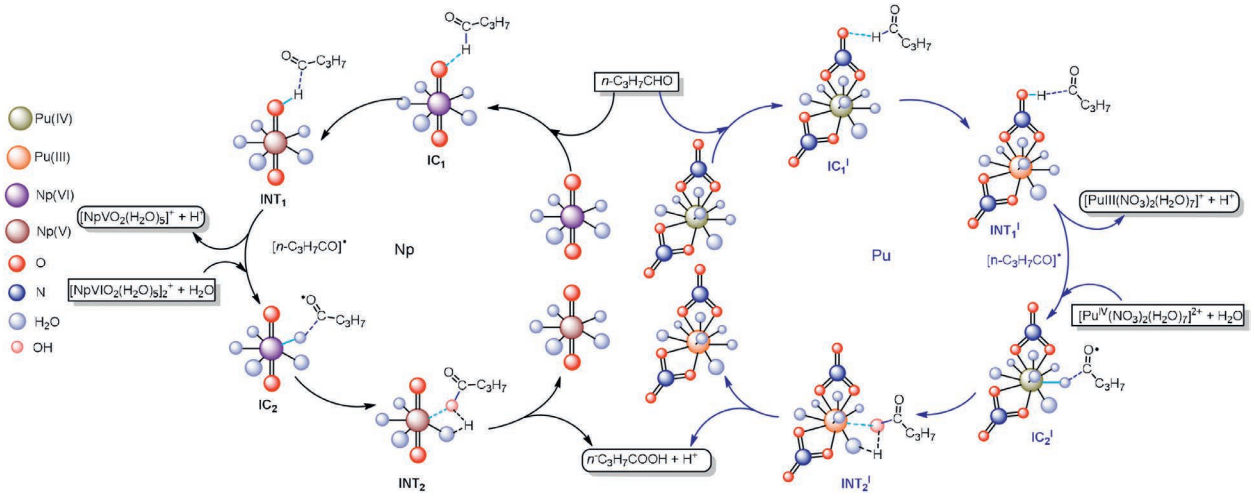
$$2M^{2+} + n\text{-}C_3H_7CHO + H_2O = 2M^{+} + n\text{-}C_3H_7COOH + 2H^{+}$$

$$(M = [NpO_2(H_2O)_5] \text{ or } [Pu(NO_3)_2(H_2O)_7]) \quad (1)$$

$$M^{2+} + n\text{-}C_3H_7CHO \rightarrow M^{+} + [n\text{-}C_3H_7CO]^{\bullet} + H^{+} \quad (2)$$

$$M^{2+} + [n\text{-}C_3H_7CO]^{\bullet} + H_2O \rightarrow M^{+} + n\text{-}C_3H_7COOH + H^{+} \quad (3)$$

The reduction processes for the Np(VI)/Pu(IV) with *n*-butyraldehyde are presented in Scheme 2. Oxygen atom of the neptunyl ion receives hydrogen atom from the aldehyde group, resulting in the generation of the free radical [*n*-C_3H_7CO]$^{\bullet}$ as well as Np(V) in the process of the first Np(VI) reduction (Eq. 2). Subsequently, the carbon atom of the aldehyde group in [*n*-C_3H_7CO]$^{\bullet}$ contacts with the oxygen atom of the water molecule coordinated with the neptunyl ion, which accomplishes the reduction of the second Np(VI), and finally obtains Np(V) and *n*-butyric acid (*n*-C_3H_7COOH) with the help of a water molecule (Eq. 3). For the Pu(IV) reduction by *n*-butyraldehyde, the hydrogen atom of the aldehyde group migrates to the oxygen atom of the nitrate ion and forms Pu(III) and [*n*-C_3H_7CO]$^{\bullet}$, which enables the first Pu(IV) reduction. Next, carbon atom of the aldehyde group in [*n*-C_3H_7CO]$^{\bullet}$ touches the oxygen atom of a water molecule, which facilitates the second Pu(IV) reduction.



Scheme 2. Reaction processes for the reduction of Np(VI) (left) and Pu(IV) (right) with *n*-butyraldehyde.

The structures and PEP for the Np(VI) reduction by *n*-butyraldehyde are shown in Fig. 1. Firstly, n-C_3H_7CHO with $[Np^{VI}O_2(H_2O)_5]^{2+}$ forms IC1 by vdW interaction using IGMH (Fig. S3 in Supporting information), which is an endothermic process (2.60 kcal/mol). In IC1, the C–O and C–H bonds are 1.220 and 1.110 Å, respectively, and both the Np-O_{yl1} and Np-O_{yl2} bonds are 1.738 Å, which are almost the same with the corresponding bond distances in the isolated n-C_3H_7CHO molecule and $[Np^{VI}O_2(H_2O)_5]^{2+}$ as presented in Fig. S2. The bond distance of Np-O_{yl} in $[Np^{V}O_2(H_2O)_5]^{+}$ and $[Np^{VI}O_2(H_2O)_5]^{2+}$ is 1.800 Å and 1.738 Å, respectively, reflecting that the bond distance of Np-O_{yl} is sensitive to the valence state of Np. The transition from IC1 to INT1 requires overcoming TS1 with the energy barrier of 18.43 kcal/mol. TS1 has an imaginary frequency with the value of 1247.51i cm^{-1}, which corresponds to vibrational motion associated with the hydrogen atom between the C and O_{yl1} atoms. The C–H and O_{yl1}–H bond distances significantly change from IC1 to INT1, which verifies the cleavage of the C–H bond and the concomitant formation of the O_{yl1}–H bond. At the same time, the Np-O_{yl1} bond distance greatly increases from 1.738 Å in IC1 to 1.968 Å in INT1, indicating that the valence state of Np changes from Np(VI) in IC1 to Np(V) in INT1. The C–O bond distance is 1.189 Å in INT1, which is comparable to that in $[n$-$C_3H_7CO]^{\bullet}$ (1.195 Å, Fig. S2), revealing that n-C_3H_7CO fragment in INT1 has free radical character. According to the results discussed above, the first reduction of Np(VI) can be attributed to the hydrogen atom transfer of the aldehyde group [84,85]. INT1 decomposes into free radical $[n$-$C_3H_7CO]^{\bullet}$, $[Np^{V}O_2(H_2O)_5]^{+}$, and H^+. Moreover, we also considered another case that the H atom of the aldehyde group contacts the oxygen atom of the coordinated water molecule, as shown in Fig. S4 (Supporting information). Clearly, the energy barrier for this process (35.83 kcal/mol) is significantly higher than that for H atom transfer to the O_{yl} atom (18.43 kcal/mol), which indicates that the H atom of the aldehyde group preferentially interacts with the O_{yl} atom.

$[n$-$C_3H_7CO]^{\bullet}$ combines with another $[Np^{VI}O_2(H_2O)_5]^{2+}$, resulting in the formation of IC2, which is a significantly exothermic process. In IC2, the carbon atom of the aldehyde group and the oxygen atom (O_{W1}) of the water molecule form the C–O_{W1} bond with the distance of 2.480 Å, which leads to the longer Np-O_{W1} bond distance (2.651 Å) compared to the average Np-O_W bond distance in $[Np^{V}O_2(H_2O)_5]^{+}$ (2.544 Å) and $[Np^{VI}O_2(H_2O)_5]^{2+}$ (2.445 Å). The Np-O_{yl1} and Np-O_{yl2} bond distances are close to 1.800 Å in IC2, which suggests that Np(VI) is immediately reduced to Np(V) as soon as $[n$-$C_3H_7CO]^{\bullet}$ contacts with $[Np^{VI}O_2(H_2O)_5]^{2+}$. The transition from IC2 to INT2 involves a slightly endothermic process with the energy of 1.24 kcal/mol, requiring overcoming 4.23 kcal/mol energy barrier. The C–O_{W1} bond distance significantly decreases from 2.480 Å in IC2 to 1.489 Å in INT2, at the same time, the Np-O_{W1} bond increases from 2.651 Å in IC2 to 2.873 Å in TS2 and completely disappears in INT2. Noticeably, this process accompanies the elongation of the O_{W1}–H_W bond and the shortening of the O_{W2}–H_W bond due to the change of the C–O_{W1} bond distance. The structural feature makes the second Np(VI) susceptible to reduction. Finally, INT2 decomposes into n-C_3H_7COOH and $[Np^{V}O_2(H_2O)_5]^{+}$, along with the release of H^+. In total, although the energy barrier for the reduction of the first Np(VI) (18.43 kcal/mol) is considerably larger than that for the reduction of the second Np(VI) (4.23 kcal/mol), both reduction processes are still kinetically feasible. Moreover, the energy change for the reduction of Np(VI) using *n*-butyraldehyde is −32.84 kcal/mol. These results indicate that the reduction of Np(VI) by *n*-butyraldehyde is both thermodynamically and kinetically feasible. In addition, the gap between the lowest unoccupied molecular orbital (LUMO) and singly occupied molecular orbital (SOMO) of IC1 complex is 2.17 eV, which is smaller than that of IC2 (3.55 eV), as presented in Fig. S5 (Supporting information), while the trend of the corresponding energy barrier is inverse. It shows that the larger value of the SOMO-LUMO gap, the smaller the energy barrier.

The assessment of the oxidation state in metal ions can be enabled by spin density [86]. Fig. 2 illustrates the spin density diagrams of ICs, TSs, and INTs structures and the spin density value of Np atom. Table S1 (Supporting information) lists the spin density values on H, C, O, and Np atoms. The spin density value of Np atom in $[Np^{VI}O_2(H_2O)_5]^{2+}$ is 1.170 a.u., while that in $[Np^{V}O_2(H_2O)_5]^{+}$ is 2.172 a.u., as depicted in Fig. S6 (Supporting information). These values are close to the corresponding formal spin density values of 1 and 2, respectively, confirming that the theoretical approach we used here is reliable for the Np complexes. The spin density value of Np atom in IC1 (1.260 a.u.) is comparable to that in $[Np^{VI}O_2(H_2O)_5]^{2+}$, which implies the valence state of Np(VI) in IC1. The value in INT1 significantly increases to 2.161 a.u., nearly equivalent to the value observed in $[Np^{V}O_2(H_2O)_5]^{+}$, indicating the valence state of Np(V) in INT1. In addition, the total spin density value of O, C, and H atoms of the n-C_3H_7CHO fragment in IC1 is 0, while it sharply increases to 0.897 a.u. in INT1, illuminating the free radical character of n-C_3H_7CO fragment in INT1. Therefore, the reduction of the first Np(VI) results in the formation of Np(V) and $[n$-$C_3H_7CO]^{\bullet}$, which can be ascribed to the hydro-

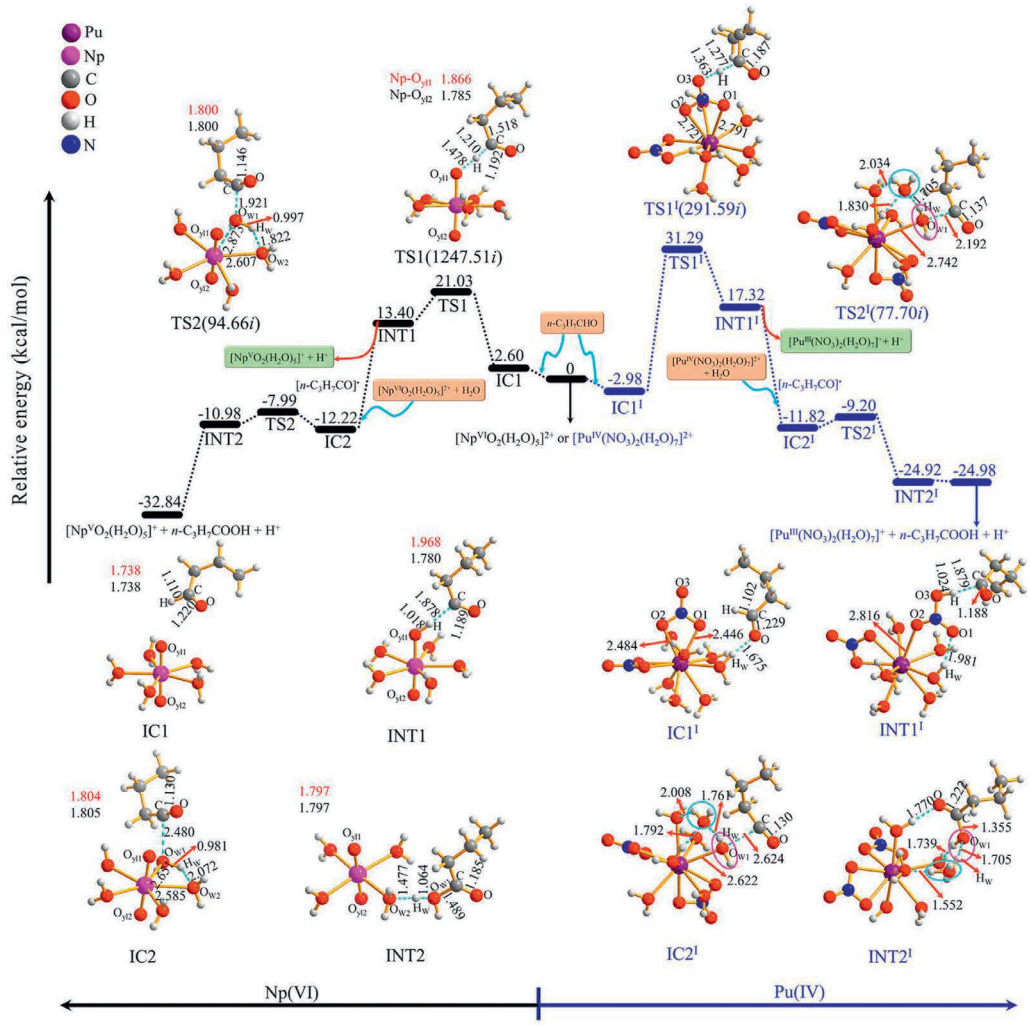


Fig. 1. PEPs of the reduction of Np(VI)/Pu(IV) with n-C_3H_7CHO at the B3LYP-SO/TZ2P level of theory in the aqueous phase. The structures, the related bond distances (Å), and imaginary frequencies (cm^{-1}) of TSs (shown in parentheses) are presented at the B3LYP/ECP60MWB/6–31G(d) level of theory. O_{yl1} and O_{yl2} represent oxygen atoms of neptunyl ion that participated and unparticipated in the Np(VI) reduction, respectively. O3, O2, and O1 atoms represent the oxygen atoms within the nitrate ion. H_W and O_W correspond to hydrogen and oxygen atoms of the water molecule, respectively.

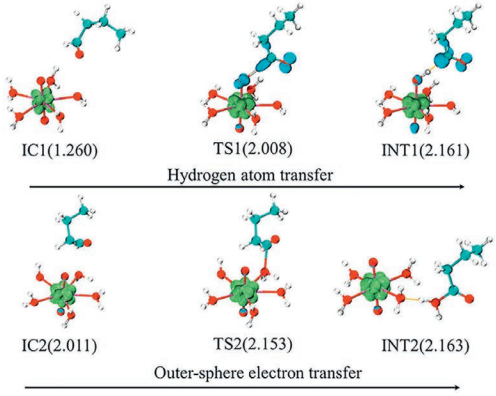


Fig. 2. Diagrams of spin density in the ICs, TSs, and INTs structures (isovalue = 0.02) as well as the spin density value for Np atom. White, red, cyan, mauve balls correspond to H, O, C, and Np atoms, respectively.

gen atom transfer of the aldehyde group. The value of spin density for Np atom across the IC2, TS2, and INT2 structures ranges from ∽2.01 a.u. to 2.16 a.u., indicating that Np(V) valence state in these structures. Furthermore, the sum of spin densities for the C and O atoms of [n-C_3H_7CO]• fragment in the structures of IC2, TS2, and INT2 is close to 0, showing the disappearance of free radical character for [n-C_3H_7CO]•, as presented in Fig. 2. These results suggest that the reduction of the second Np(VI) is promptly accomplished when [n-C_3H_7CO]• contacts with Np(VI). So the reduction of the second Np(VI) is the outer-sphere electron transfer, which can be supported by previous works [87–89]. Therefore, the reduction nature for the first and second Np(VI) is characterized by hydrogen atom transfer and outer-sphere electron transfer, respectively.

LMO analysis has been employed to uncover the bonding characteristics and illuminate the process of the chemical reaction [90,91]. Diagrams and the corresponding atomic contribution of LMOs for the structures of Np(VI) reduction by n-butyraldehyde are shown in Fig. 3 and Fig. S7 (Supporting information). For the reduction process of the first Np(VI) from IC1 to INT1, the C–H σ LMO disappears and a new O_{yl1}–H σ LMO forms (Fig. S7). The diagrams of LMOs in Fig. 3 also reflect that the Np-O_{W1} σ LMO gradually disappears and C–O_{W1} σ LMO progressively forms from IC2 to INT2, which results in the obvious change of the contribution for the out-of-plane C–O π LMO. That is, the contribution of C atom decreases from 28.7% in IC2 to 14.9% in INT2 for the out-of-plane C–O π LMO, while the corresponding contribution of C atom for

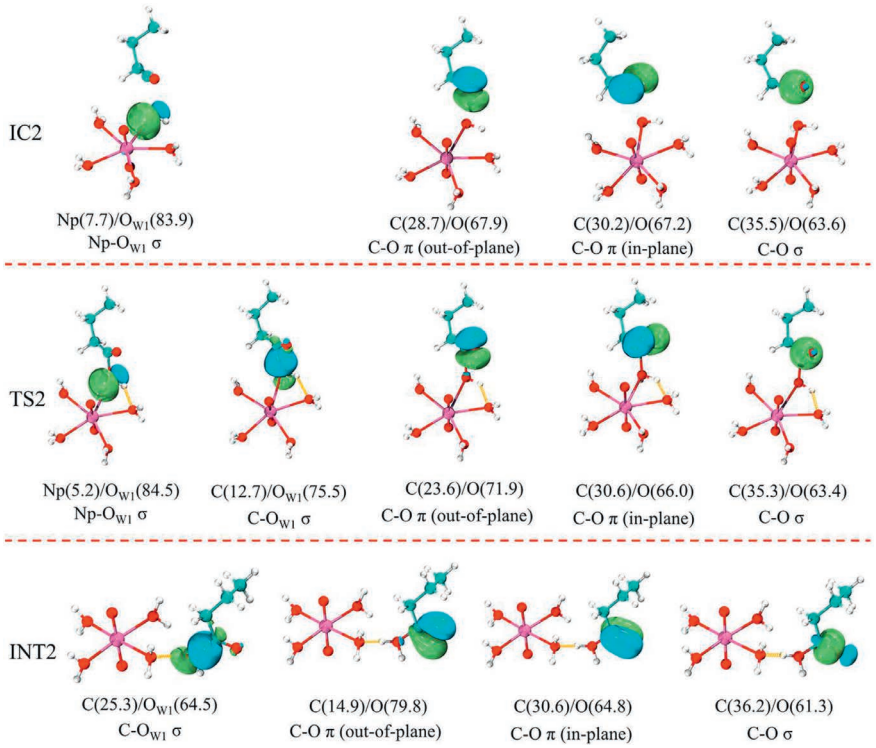


Fig. 3. Diagrams and atomic contribution (%) of LMOs (isovalue = 0.05) for IC2, TS2, and INT2 of Np(VI) reduction with *n*-butyraldehyde.

C–O σ and in-plane C–O π LMOs remains almost the same. The result indicates that the reduction of Np(VI) takes place in a certain direction of *n*-butyraldehyde [92,93]. Therefore, LMOs reflect the bonding evolution and reaction direction for the Np(VI) reduction with *n*-butyraldehyde.

It is clearly seen in Fig. 1 that $[Pu^{IV}(NO_3)_2(H_2O)_7]^{2+}$ and *n*-C_3H_7CHO form $IC1^I$ *via* the O–H_W hydrogen bond with a distance of 1.675 Å. The Pu-O1 and Pu-O2 bond distances are 2.446 and 2.484 Å in $IC1^I$, which keeps almost the same values of the $[Pu^{IV}(NO_3)_2(H_2O)_7]^{2+}$ complex in Fig. S2. And the C–H and C–O bond distances in $IC1^I$ align well with the corresponding values of the *n*-C_3H_7CHO in Fig. S2, indicating that Pu(IV) is not reduced in the formation of $IC1^I$. The energy barrier for the Pu(IV) reduction reaction from $IC1^I$ to $INT1^I$ is 34.27 kcal/mol, revealing the kinetic infeasibility of Pu(IV) reduction. The C–H bond sharply increases from 1.102 in $IC1^I$ to 1.879 Å in $INT1^I$. Noticeably, the distance between O3 atom of nitrate ion and H atom of the aldehyde group in $IC1^I$ is 3.298 Å, while it is 1.363 Å and 1.024 Å in $TS1^I$ and $INT1^I$, respectively, indicating the formation of O3-H bond. In addition, the Pu-O1 bond increases from 2.446 Å in $IC1^I$ to 2.791 Å in $TS1^I$, and it is completely broken in $INT1^I$. The Pu-O2 bond also increases from 2.484–2.721 Å to 2.816 Å. Therefore, the reaction from $IC1^I$ to $INT1^I$ is accompanied by the formation of the O3-H bond and the dissociation of the Pu-O1 bond, which can be attributed to hydrogen atom transfer. $INT1^I$ decomposes into $[Pu^{III}(NO_3)_2(H_2O)_7]^+$, [*n*-$C_3H_7CO$]$^\bullet$, and H^+. Similar to the Np(VI) reduction systems, the energy barrier of the reduction process for the H atom of the aldehyde group transferred to the coordinated water oxygen (39.25 kcal/mol) is higher than that to the nitrate oxygen (34.27 kcal/mol), as shown in Fig. S4 (Supporting information).

[*n*-C_3H_7CO]$^\bullet$ and $[Pu^{IV}(NO_3)_2(H_2O)_7]^{2+}$ forms $IC2^I$ *via* the C–O_{W1} hydrogen bond with the distance of 2.624 Å. The transition of $IC2^I$ to $INT2^I$ is an obvious exothermic reaction process with a small energy barrier (2.62 kcal/mol). In this process, the carbon atom of [*n*-C_3H_7CO]$^\bullet$ progressively approaches O_{W1} atom, and appears a new C–O_{W1} bond (1.355 Å) in $INT2^I$. At the same time, the Pu-O_{W1} bond completely dissociates, which leads to the fact that the coordination number of Pu(IV) ion changes from 10 in $IC2^I$ to 9 in $INT2^I$. Noticeably, H_W atom of the water molecule (labeled by the purple circle in Fig. 1) transfers to the O atom of another water molecule (labeled by the cyan circle) and forms H_3O^+ in $INT2^I$. Finally, $INT2^I$ decomposes into $[Pu^{III}(NO_3)_2(H_2O)_7]^+$ and *n*-C_3H_7COOH. In summary, the thermodynamic result shows that the reduction of Pu(IV) by *n*-butyraldehyde is energetically favorable, with the reaction energy of −24.98 kcal/mol. The higher energy barrier of the first Pu(IV) reduction compared to that of the second one indicates that the former is the rate-determining step. Moreover, the rate-determining step with the larger energy barrier (34.27 kcal/mol) indicates that the first Pu(IV) reduction with *n*-butylaldehyde is kinetically infeasible. Additionally, the SOMO-LUMO gap of $IC1^I$ is 2.53 eV, which is smaller than that of $IC2^I$ (3.17 eV), also showing that the larger value of the SOMO-LUMO gap, the smaller the energy barrier, which is similar result of the Np(VI) systems discussed above.

Overall, the first Np(VI)/Pu(IV) reduction with *n*-butylaldehyde serves as the rate-determining step for the Np(VI)/Pu(IV) reduction. Based on the energy barrier of the rate-determining step, *n*-butylaldehyde is more kinetically favorable for the reduction of Np(VI) compared to that of Pu(IV), which explains the experiment observations of fast reduction rate of Np(VI) [32]. The reaction energies for the reduction of Np(VI) and Pu(IV) are −32.84 and −24.98 kcal/mol, respectively, demonstrating that both reduction reactions are thermodynamically favorable. Therefore, the selective reduction of Np(VI) with *n*-butylaldehyde is probably attributed to kinetic control. Interestingly, the kinetically controlled reaction has been applied to the separation of inert gas [94], *Z*/*E*-isomers [95,96], nickel(II)/cobalt(II) [97–99], and so on. Yu *et al.* found that a calcium-based metal-organic framework exhibits excellent kinetic selectivity for xenon over krypton [94]. Nguyen *et al.* obtained pure *E*-alkenyl chlorides/fluorides *via* kinetically controlled *E*-selective catalytic olefin metathesis [95]. The separation

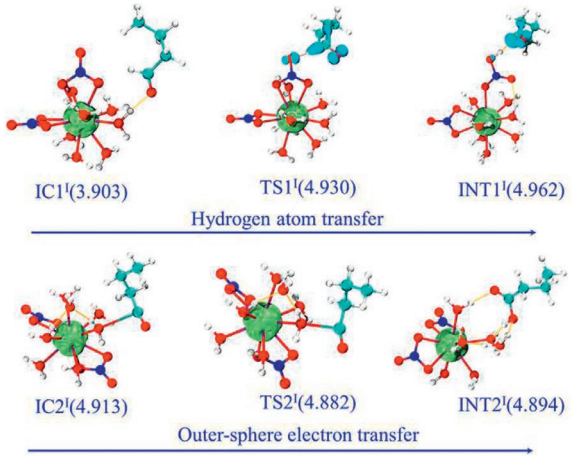


Fig. 4. Diagrams of spin density in the ICs^{I}, TSs^{I}, and INTs^{I} structures (isovalue = 0.02) and the spin density value for Pu atom in the reduction of Pu(IV) with *n*-butyraldehyde. White, blue, red, cyan, and purple balls correspond to H, N, O, C, and Pu atoms, respectively.

of nickel(II)/cobalt(II) was achieved by using 5-octyloxymethyl-8-quinolinol based on the different extraction kinetics [97]. In this study, we elucidate the selective reduction of Np(VI) with *n*-butylaldehyde thanks to the kinetic control based on the kinetic and thermodynamic results.

The diagrams of spin density in the ICs^{I}, TSs^{I}, and INTs^{I} structures and the value of spin density for the corresponding atoms are illustrated in Fig. 4 and Table S2 (Supporting information). The value of spin density for the Pu atom in $[Pu^{IV}(NO_3)_2(H_2O)_7]^{2+}$ and $[Pu^{III}(NO_3)_2(H_2O)_7]^{+}$ is 4.209 and 5.061 a.u. as listed in Fig. S6 (Supporting information), respectively, which is close to the formal spin density values of 4 and 5, suggesting that the level of theory employed in this study is also suitable to the Pu complexes. The spin density value on Pu atom is 3.903 a.u. in IC1^{I}, while it changes to about 5.0 a.u. in both TS1^{I} and INT1^{I}. Moreover, the value of total spin density for the H, C, and O atoms in *n*-C_3H_7CHO fragment obviously increases from 0 in IC1^{I} to 0.964 a.u. in INT1^{I}, reflecting free radical character in the latter. These results indicate that the reduction process of the Pu(IV) to Pu(III) is accompanied by the formation of Pu(III) and [*n*-C_3H_7CO]$^{\bullet}$. The value of spin density on Pu atom in the IC2^{I}, TS2^{I}, and INT2^{I} structures is approximately 4.9 a.u., indicating that the oxidation state of Pu in these structures is Pu(III). Furthermore, the value of spin density associated with the C and O atoms of *n*-C_3H_7CO fragment in IC2^{I}, TS2^{I}, and INT2^{I} approaches 0, indicating that its free radical character disappears, which can be clearly seen in Fig. 4. These results reflect that the second Pu(IV) is rapidly reduced to Pu(III) when [*n*-C_3H_7CO]$^{\bullet}$ contacts with Pu(IV), suggesting that the reduction of the second Pu(IV) is outer-sphere electron transfer. All in all, the reduction nature of Np(VI)/Pu(IV) with *n*-C_3H_7CHO is hydrogen atom transfer and outer-sphere electron transfer, which varies from the Pu(IV)/Np(VI) reduction with methylhydrazine in previous works [41,43]. These results highlight the different reduction behaviors of Np(VI)/Pu(IV) by using different types of reductants, which may be attributed to their electronic structures and functional groups.

Fig. S8 (Supporting information) shows the C–H, Pu-O1, and Pu-O2 σ LMOs in IC1^{I}, while they disappear and O3-H σ LMO is formed in INT1^{I}. Fig. 5 presents the disappearance of the Pu-O_{W1} σ LMO and the emergence of C–O_{W1} π and σ LMOs from IC2^{I} to INT2^{I}. At the same time, the contribution of C atom decreases for out-of-plane C–O π LMO orbital. Therefore, LMOs diagrams elucidate the progressive bonding changes during the process of Pu(IV) reduction with *n*-butyraldehyde.

The reaction processes of *n*-butyraldehyde with Pu(IV) and Np(VI) were investigated using relativistic density functional calculations. According to the potential energy profiles, the rate-determining step is the first Pu(IV)/Np(VI) reduction with energy barriers of 34.27 and 18.43 kcal/mol, respectively, which implies that the Np(VI) reduction by *n*-butyraldehyde is preferred kinetically, while the Pu(IV) reduction is kinetically infeasible. The negative reaction energy of Pu(IV)/Np(VI) with *n*-butyraldehyde suggests that both Pu(IV) and Np(VI) reductions are thermodynamically favorable. Therefore, the efficiently selective reduction of Np(VI) by *n*-butyraldehyde thanks to the kinetic control. Analyses of the spin density and bond distance show that the first Pu(IV)/Np(VI) reduction occurs through hydrogen atom transfer, whereas the second one corresponds to the outer-sphere electron transfer. LMO analysis clearly illustrates the bonding evolution of the reduction process of the Pu(IV)/Np(VI) with *n*-butyraldehyde. This study elucidates the reduction nature and mechanisms of Pu(IV)/Np(VI) with *n*-butyraldehyde using theoretical approaches and explains the reason that selective reduction of Np(VI) by *n*-butyraldehyde, which can provide theoretical guidance for the selective reduction of Pu(IV)/Np(VI) in SNF. Moreover, this work offers new inspirations for effectively adjusting the oxidation states

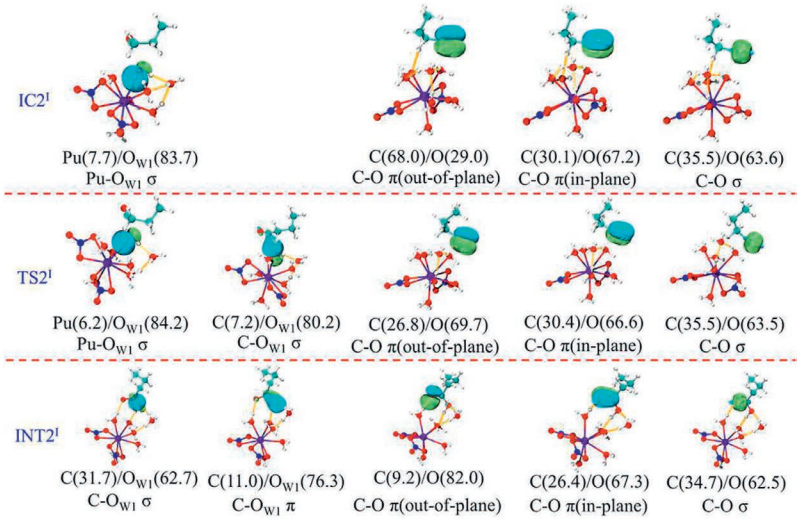


Fig. 5. Diagrams and atomic contribution (%) of LMOs (isovalue = 0.05) of IC2^{I}, TS2^{I}, and INT2^{I} during the reduction of Pu(IV) by *n*-butyraldehyde.

of specific metal ions to achieve their separation based on kinetic control.

Declaration of competing interest

The authors declare that they have no known competing financial interests or personal relationships that could have appeared to influence the work reported in this paper.

CRediT authorship contribution statement

Xiaobo Li: Writing – original draft, Formal analysis, Data curation. **Qunyan Wu:** Funding acquisition, Data curation, Writing – review & editing, Conceptualization. **Congzhi Wang:** Methodology. **Jianhui Lan:** Methodology. **Meng Zhang:** Supervision. **Weiqun Shi:** Supervision, Funding acquisition, Writing – review & editing.

Acknowledgment

This work was supported by the National Natural Science Foundation of China (Nos. 22376197, U2441225, 22076188).

Supplementary materials

Supplementary material associated with this article can be found, in the online version, at doi:10.1016/j.cclet.2025.111503.

References

[1] Y. Liu, X.P. Shao, W.T. Bu, et al., Chin. Chem. Lett. 33 (2022) 3384–3394.
[2] T.Y. Xiu, S.M. Zhang, P. Ren, et al., Chin. Chem. Lett. 34 (2023) 108440.
[3] W.X. Xiao, D.Q. Pan, Z.W. Niu, et al., Chin. Chem. Lett. 33 (2022) 3413–3421.
[4] L.K. Liu, S.B. Xie, H.B. Lv, et al., Chin. Chem. Lett. 33 (2022) 3439–3443.
[5] O. Artun, Appl. Radiat. Isotopes 166 (2020) 109337.
[6] X. Zhang, L. Zhang, T. Bo, et al., Chin. Chem. Lett. 33 (2022) 3527–3530.
[7] X.H. Kong, X.L. Liao, Z.K. Huang, et al., Chin. Chem. Lett. 35 (2024) 109642.
[8] R.E. Isaacson, B.F. Judson, Ind. Eng. Chem. Process Des. Dev. 3 (1964) 296–301.
[9] M. Benedict, T.H. Pigford, H.W. Levi, Nuclear Chemical Engineering, 2nd ed., McGraw-Hill Education, New York, 1981.
[10] K.W. Kim, K.C. Song, E.H. Lee, et al., J. Radioanal. Nucl. Chem. 246 (2000) 215–219.
[11] X. Dong, Z.P. Wang, Q. Yan, et al., Chin. Chem. Lett. 33 (2022) 3531–3533.
[12] S.L. Yarbro, S.B. Schreiber, E.M. Ortiz, et al., J. Radioanal. Nucl. Chem. 235 (1998) 21–25.
[13] V.S. Koltunov, S.M. Baranov, Radiochemistry 42 (2000) 236–241.
[14] A.Y. Zhang, J.X. Hu, X.Y. Zhang, et al., J. Radioanal. Nucl. Chem. 253 (2002) 107–113.
[15] Y.X. Chen, H.B. Tang, J.P. Liu, et al., J. Radioanal. Nucl. Chem. 289 (2011) 41–47.
[16] V.I. Marchenko, K.N. Dvoeglazov, O.A. Savilova, et al., Radiochemistry 54 (2012) 459–464.
[17] T.H. Yan, W.F. Zhen, G.A. Ye, et al., J. Radioanal. Nucl. Chem. 279 (2009) 293–299.
[18] T.H. Yan, W.F. Zheng, C. Zuo, et al., Radiochim. Acta 98 (2010) 35–38.
[19] P. Sivakumar, S. Meenakshi, R.V.S. Rao, J. Radioanal. Nucl. Chem. 292 (2012) 603–608.
[20] V.S. Koltunov, R.J. Taylor, S.M. Baranov, et al., Radiochim. Acta 88 (2000) 65–70.
[21] V.S. Koltunov, S.M. Baranov, V.G. Pastushchak, Radiochemistry 43 (2001) 346–349.
[22] V.S. Koltunov, E.A. Mezhov, S.M. Baranov, Radiochemistry 43 (2001) 342–345.
[23] V.S. Koltunov, R.J. Taylor, S.M. Baranov, et al., J. Nucl. Sci. Technol. 39 (2002) 878–881.
[24] V.S. Koltunov, S.M. Baranov, Inorg. Chim. Acta 140 (1987) 31–34.
[25] X.Y. Zhang, Z.L. Huang, S.T. Xiao, et al., Atomic Energy Science Technology 33 (1999) 8–11.
[26] V. Koltunov, J. Nucl. Sci. Technol. 39 (2002) 347–350.
[27] V.S. Koltunov, K.M. Frolov, Y.V. Isaev, Radiochemistry 44 (2002) 121–126.
[28] W.Q. Shi, H.B. Tang, Y.X. Ye, et al., J. Nucl. Radiochem. 24 (2002) 134–137.
[29] Y. Ban, T. Asakura, Y. Morita, J. Radioanal. Nucl. Chem. 279 (2009) 423–429.
[30] H. Yang, H. Zhang, L. Li, et al., Nuclear Techniques 39 (2016) 37–44.
[31] Z.Y. Liu, H. Zhang, R.T. Wang, et al., Nuclear Techniques 40 (2017) 28–34.
[32] G. Uchiyama, S. Fujine, S. Hotoku, et al., Nucl. Technol. 102 (1993) 341–352.
[33] G. Uchiyama, S. Hotoku, S. Fujine, et al., Nucl. Technol. 122 (1998) 222–227.
[34] G. Uchiyama, H. Mineo, S. Hotoku, et al., Prog. Nucl. Energy 37 (2000) 151–156.
[35] V.I. Marchenko, V.S. Koltunov, O.A. Savilova, et al., Radiochemistry 43 (2001) 276–283.
[36] Y. Ban, T. Asakura, Y. Morita, Radiochim. Acta 92 (2004) 883–887.
[37] Z.P. Cheng, Q.Y. Wu, Y.H. Liu, et al., RSC Adv. 6 (2016) 109045–109053.
[38] X.B. Li, Q.Y. Wu, C.Z. Wang, et al., J. Phys. Chem. A 124 (2020) 3720–3729.
[39] X.B. Li, Q.Y. Wu, C.Z. Wang, et al., J. Phys. Chem. A 125 (2021) 6180–6188.
[40] Z.P. Cheng, X.B. Li, Q.Y. Wu, et al., Radiochim. Acta 110 (2022) 471–480.
[41] X.B. Li, Q.Y. Wu, C.Z. Wang, et al., Phys. Chem. Chem. Phys. 24 (2022) 17782–17791.
[42] X.B. Li, Q.Y. Wu, C.Z. Wang, et al., J. Phys. Chem. A 127 (2023) 4259–4268.
[43] X.B. Li, Q.Y. Wu, C.Z. Wang, et al., Chin. Chem. Lett. 35 (2024) 109359.
[44] X. Huang, X.B. Li, Q.Y. Wu, et al., Phys. Chem. Chem. Phys. 26 (2024) 27395–27405.
[45] X.B. Li, Q.Y. Wu, C.Z. Wang, et al., J. Phys. Chem. A 127 (2023) 7479–7486.
[46] C.T. Lee, W.T. Yang, R.G. Parr, Phys. Rev. B 37 (1988) 785–789.
[47] A.D. Becke, J. Chem. Phys. 98 (1993) 5648–5652.
[48] Y.T. Bi, Z. Bao, L. Li, et al., ChemistrySelect 3 (2018) 4804–4810.
[49] J.P. Wang, W.Y. Xie, W.R. Jiang, et al., Adv. Theory Simul. 2 (2019) 1900138.
[50] Y.X. Wang, S.X. Hu, L.W. Cheng, et al., CCS Chem. 2 (2020) 425–431.
[51] P. Zhang, Y.X. Wang, P. Zhang, et al., Inorg. Chem. 59 (2020) 11953–11961.
[52] X.K. Zhao, C.S. Cao, J.C. Liu, et al., Chem. Sci. 13 (2022) 8518–8525.
[53] X.P. Lei, Q.Y. Wu, C.Z. Wang, et al., Inorg. Chem. 62 (2023) 2705–2714.
[54] L.L. Su, Q.Y. Wu, C.Z. Wang, et al., Chin. Chem. Lett. 35 (2024) 109402.
[55] M. Cossi, N. Rega, G. Scalmani, et al., J. Comput. Chem. 24 (2003) 669–681.
[56] V. Barone, M. Cossi, J. Phys. Chem. A 102 (1998) 1995–2001.
[57] M.J. Frisch, G.W. Trucks, H.B. Schlegel, et al., Gaussian 16 Software Program, Gaussian Inc., Wallingford, CT, 2016.
[58] W. Küchle, M. Dolg, H. Stoll, et al., J. Chem. Phys. 100 (1994) 7535–7542.
[59] X.Y. Cao, M. Dolg, H. Stoll, J. Chem. Phys. 118 (2003) 487–496.
[60] X.Y. Cao, M. Dolg, J. Mol. Struc. (THEOCHEM) 673 (2004) 203–209.
[61] E. Fromager, V. Vallet, B. Schimmelpfennig, et al., J. Phys. Chem. A 109 (2005) 4957–4960.
[62] J.K. Gibson, W.A. de Jong, P.D. Dau, et al., J. Phys. Chem. A 121 (2017) 9156–9162.
[63] J. Autschbach, J. Chem. Theory Comput. 13 (2017) 710–718.
[64] E. Van Lenthe, E.J. Baerends, J. Comput. Chem. 24 (2003) 1142–1156.
[65] C. Fonseca Guerra, J.G. Snijders, G. te Velde, et al., Theor. Chem. Acc. 99 (1998) 391–403.
[66] G. te Velde, F.M. Bickelhaupt, E.J. Baerends, et al., J. Comput. Chem. 22 (2001) 931–967.
[67] E.J. Baerends, T. Ziegler, A.J. Atkins, et al., ADF2022, Theoretical Chemistry, Vrije Universiteit, Amsterdam, The Netherlands, 2022 URL http://www.scm.com .
[68] A. Klamt, G. Schüürmann, J. Chem. Soc., Perkin Trans. 2 (1993) 799–805.
[69] A. Klamt, J. Phys. Chem. 99 (1995) 2224–2235.
[70] A. Klamt, V. Jonas, J. Chem. Phys. 105 (1996) 9972–9981.
[71] J. Pipek, P.G. Mezey, J. Chem. Phys. 90 (1989) 4916–4926.
[72] T. Lu, F.W. Chen, J. Comput. Chem. 33 (2012) 580–592.
[73] T. Lu, J. Chem. Phys. 161 (2024) 082503.
[74] T. Lu, Q.X. Chen, J. Comput. Chem. 43 (2022) 539–555.
[75] D.Kirk Veirs, C.A. Smith, J.M. Berg, et al., J. Alloys Compd. 213-214 (1994) 328–332.
[76] P.G. Allen, D.K. Veirs, S.D. Conradson, et al., Inorg. Chem. 35 (1996) 2841–2845.
[77] S.D. Conradson, K.D. Abney, B.D. Begg, et al., Inorg. Chem. 43 (2004) 116–131.
[78] A.M. Lines, S.R. Adami, S.I. Sinkov, et al., Anal. Chem. 89 (2017) 9354–9359.
[79] C. Madic, G.M. Begun, D.E. Hobart, et al., Inorg. Chem. 23 (1984) 1914–1921.
[80] P.J. Hay, R.L. Martin, G. Schreckenbach, J. Phys. Chem. A 104 (2000) 6259–6270.
[81] P. Lindqvist-Reis, C. Apostolidis, O. Walter, et al., Dalton Trans. 42 (2013) 15275–15279.
[82] L. Zhang, S.Y. Liu, Z.G. Zhao, et al., Chem. Sci. 9 (2018) 6085–6090.
[83] L.Y. Wang, Y.B. Zhang, J. Yao, et al., Catal. Lett. 152 (2022) 1131–1139.
[84] J.R. Bryant, J.M. Mayer, J. Am. Chem. Soc. 125 (2003) 10351–10361.
[85] J.M. Mayer, Acc. Chem. Res. 44 (2011) 36–46.
[86] K.R. Gorantla, B.S. Mallik, J. Phys. Chem. A 126 (2022) 3301–3310.
[87] J.G. Muller, R.P. Hickerson, R.J. Perez, et al., J. Am. Chem. Soc. 119 (1997) 1501–1506.
[88] R.S. Miller, J.M. Sealy, M. Shabangi, et al., J. Am. Chem. Soc. 122 (2000) 7718–7722.
[89] Y.M. Lee, S. Kim, K. Ohkubo, et al., J. Am. Chem. Soc. 141 (2019) 2614–2622.
[90] Y. Wakatsuki, N. Koga, H. Werner, et al., J. Am. Chem. Soc. 119 (1997) 360–366.
[91] R.Z. Sun, M.Y. Yu, G.Q. Luo, et al., Chem. Eng. J. 407 (2021) 127113.
[92] J.L. Qu, J.W. Xiao, H.T. Chen, et al., Chin. J. Catal. 42 (2021) 288–296.
[93] F.Z. Zhang, Q.P. Kong, H.H. Chen, et al., Chem. Eng. J. 434 (2022) 134674.
[94] G.L. Yu, Y.Q. Liu, X.Q. Zou, et al., J. Mater. Chem. A 6 (2018) 11797–11803.
[95] T.T. Nguyen, M.J. Koh, X. Shen, et al., Science 352 (2016) 569–575.
[96] X. Shen, T.T. Nguyen, M.J. Koh, et al., Nature 541 (2017) 380–385.
[97] H. Kokusen, K. Suzaki, K. Ohashi, et al., Anal. Sci. 4 (1988) 617–622.
[98] K.E. Mayhew, T.M. McCoy, D.L. Jones, et al., Solvent Extr. Ion Exch. 29 (2011) 755–781.
[99] Y.Y. Liang, L. Mei, Q.Y. Jin, et al., Chin. Chem. Lett. 33 (2022) 3539–3542.